



Analysis and simulation of scale-up potentials in reverse electrodialysis

Michele Tedesco^a, Paolo Mazzola^a, Alessandro Tamburini^a, Giorgio Micale^a,
I. David L. Bogle^b, Michael Papapetrou^c, Andrea Cipollina^{a,*}

^aDipartimento di Ingegneria Chimica, Gestionale, Informatica, Meccanica (DICGIM), Università di Palermo (UNIPA), Viale delle Scienze Ed. 6, 90128 Palermo, Italy, email: andrea.cipollina@unipa.it (A. Cipollina)

^bCentre for Process Systems Engineering, Department of Chemical Engineering, University College London (UCL), London WC1E 7JE, UK

^cWirtschaft und Infrastruktur GmbH & Co Planungs-KG (WIP), Sylovensteinstr. 2, 81369 Munich, Germany

Received 19 April 2014; Accepted 16 June 2014

ABSTRACT

The reverse electrodialysis (RED) process has been widely accepted as a viable and promising technology to produce electric energy from salinity difference (salinity gradient power e.g. using river water/seawater or seawater and concentrated brines). Recent R&D efforts demonstrated how an appropriate design of the RED unit and a suitable selection of process conditions may crucially enhance the process performance. With this regard, a process simulator was developed and validated with experimental data collected on a laboratory-scale unit, providing a new modelling tool for process optimisation. In this work, performed within the REAPower project (www.reapower.eu), a process simulator previously proposed by the same authors has been modified in order to predict the behaviour of a cross-flow RED unit. The model was then adopted to investigate the influence of the most important variables (i.e. solution properties and stack geometry) on the overall process performance. In particular, the use of different concentrations and flow rates for the feed streams has been considered, as well as different aspect ratios in asymmetric stacks. Moreover, the influence of the scaling-up a RED unit was investigated, starting from a $22 \times 22 \text{ cm}^2$ 100 cell pairs lab-stack, and simulating the performance of larger stacks up to a $44 \times 88 \text{ cm}^2$ 500 cell pairs unit. Finally, different scenarios are proposed for a prototype-scale RED plant, providing useful indications for the technology scale-up towards 1 kW of power production, relevant to the installation of a real prototype plant in Trapani (Italy) being the final objective of the R&D activities of the REAPower project.

Keywords: Salinity gradient power; RED; Sea water; Brine; Process simulator; Model

1. Introduction

Among the novel renewable energy sources investigated nowadays, a growing interest is being gained

by salinity gradient power (SGP), i.e. the energy available from the mixing of two aqueous solutions with different salinities. SGP has been estimated to be the second largest marine-based energy source, with a global power of 980 GW potentially available for

*Corresponding author.

*Presented at the Conference on Desalination for the Environment: Clean Water and Energy
11–15 May 2014, Limassol, Cyprus*

2. Description of the modelling approach

A multi-scale modelling approach has been applied to describe the system (Fig. 2) [21]. According to this method, a lower scale model describes the physical phenomena in a single repeating unit of the stack (*cell pair*). The second level of description refers to the whole *stack*, including all cell pairs and the relevant interconnections. Finally, a *plant* model has been implemented, allowing to simulate more stacks connected with different layouts.

2.1. Model development and implementation

A model for RED process using sea/brackish water as diluate and brines as concentrate streams was already presented by the authors [20], aiming at a comprehensive simulation tool for the RED process accounting for all the above-mentioned non-ideal phenomena.

The complete set of model equations can be found in [20]. This paragraph illustrates only the new implementations carried out within the present work, in order to simulate the operation of a cross-flow stack with possible asymmetric configurations of the feed channels.

2.1.1. Development of a 2-D model structure to simulate cross-flow arrangement

It is worth noting that the model described in [20] was developed for a co-current flow distribution, where all the variables dependent on salt concentration (solution conductivity, cell pair voltage, etc.) vary only along compartment length. For this reason, a 1-D distributed model was considered, where the compu-

tational domain was discretised along the compartment length (Fig. 3(a)).

In this work, the previous model was purposely modified in order to account for a different flow arrangement, with cross-flow currents. In this case, the computational domain is defined in 2-D, where x and y are the flow directions for the concentrate and dilute solutions, respectively (Fig. 3(b)).

The main advantage of such 2-D model approach is the high flexibility to simulate the use of asymmetric stack geometries, with one compartment longer and the other one wider, thus changing the aspect ratio of the system.

The new computational domain required a number of modifications within the model formulation. In particular, all distributed variables described as x -dependent in [20] can vary along both x and y coordinates. Likewise, the mass balance in diluate and concentrate compartments has been modified as:

$$\frac{\partial(Q_{HIGH}C_{HIGH}(x,y))}{\partial x} = -J_{tot}(x,y) \, dy \tag{1}$$

$$\frac{\partial(Q_{LOW}C_{LOW}(x,y))}{\partial y} = J_{tot}(x,y) \, dx \tag{2}$$

$$\frac{\partial(Q_{HIGH}(x,y))}{\partial x} = -J_{w,net}(x,y) \, dy \tag{3}$$

$$\frac{\partial(Q_{LOW}(x,y))}{\partial y} = J_{w,net}(x,y) \, dx \tag{4}$$

where Q is the volumetric flow rate in each compartment, C is the molar concentration and J_{tot} and $J_{w,net}$ are the salt and solvent fluxes through membranes.

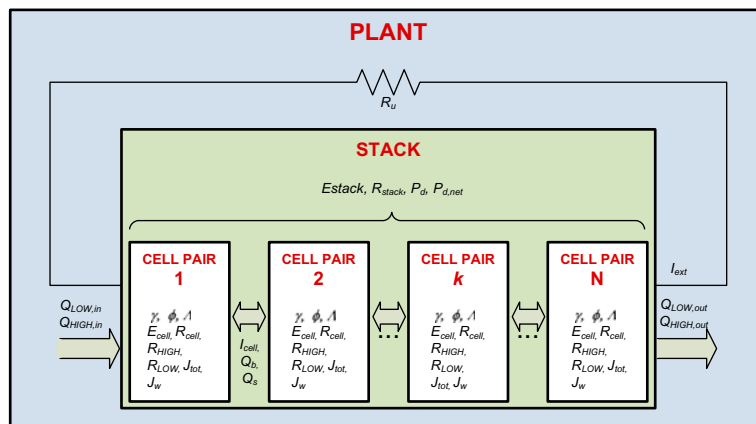


Fig. 2. Hierarchical structure of the proposed model.

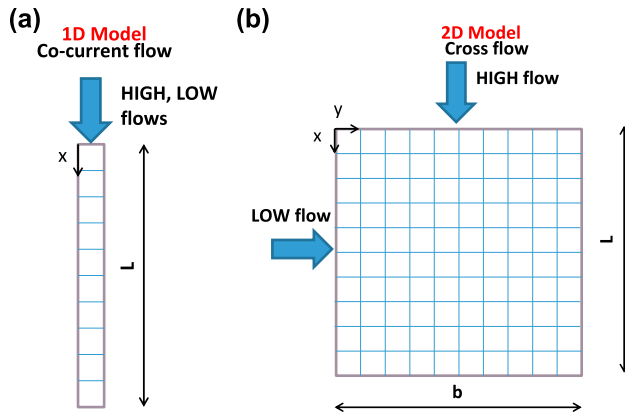


Fig. 3. Computational domain of developed models: (a) 1-D model [17]; (b) 2-D model (this work).

Subscripts *HIGH* and *LOW* refer to concentrated and dilute solutions, respectively.

2.1.2. Response variables of the process

For the sake of brevity, only the model response variables are reported. In particular, the gross power produced by the system is:

$$P = I_{ext}^2 R_u \quad (5)$$

where I_{ext} is the electric current in the external circuit and R_u is the external load connected to the stack. The required power for pumping the salt solutions through the stack is calculated by:

$$P_{pump} = \frac{\Delta P_{HIGH} Q_{HIGH}^{tot} + \Delta P_{LOW} Q_{LOW}^{tot}}{\eta_p} \quad (6)$$

where ΔP is the total pressure drop, Q^{tot} is the flow rate of both solutions and η_p is pump efficiency (assumed to be 75%); subscripts *HIGH* and *LOW* refer to concentrate and diluate, respectively. Pressure drops for both solutions were estimated based on experimentally measured data for a single channel filled with a 270 μm polyamide woven spacer [20].

The power density is defined as the electric power produced by the system per unit cell pair area and is given by:

$$P_d = \frac{1}{N} \left(\frac{I_{ext}}{A} \right)^2 R_u \quad (7)$$

where N is the number of cell pairs within the RED unit and A is the membrane active area. Finally, the net power density is given by:

$$P_{d,net} = P_d - \frac{P_{pump}}{NA} \quad (8)$$

In Eq. (8), the pumping power (P_{pump}) has been divided by the cell pair area (NA) to be dimensionally consistent with the power density.

2.2. Validation of the model on a laboratory-scale unit

The newly implemented model was validated by experimental data collected with a 50 cell pairs stack with cross-flow arrangement. Experimental tests were performed changing the inlet concentration of diluate and concentrate [20]. Results are shown in Fig. 4.

Fig. 4 shows how the model can predict with good agreement the experimental behaviour of the system in a wide range of feed concentrations.

3. Simulation results and analysis of perspectives

3.1. Comparison of 1-D and 2-D models

Unlike the 1-D model, the new one can evaluate all the relevant 2-D distributed variables on membrane surface. As an example, Fig. 5 shows the concentration profiles predicted by both models for a $20 \times 20 \text{ cm}^2$ stack equipped with 50 cell pairs.

Interestingly, the 2-D maps indicate that the main concentration variation occurs along the flow direction, which was the only one predictable by the 1-D model. However, for cross-flow stack, this variation occurs for the two solutions in perpendicular directions, as can be predicted only by a 2-D model. Moreover, a less important (yet predictable) variation in concentration occurs also in the direction perpendicular to the flow only within the diluate compartment, while a pretty mono-dimensional behaviour can be observed for the concentrate one.

As a result of the predicted change in concentrations in the two “cross-flow” channels, the variation of cell voltage along the two directions is also predicted by the 2-D model. Fig. 6 shows how the cell voltage is maximum at the origin of the x - y axis, corresponding to the inlet of both solutions, while it is minimum in the opposite corner, corresponding to the outlet of the two solutions. Also in this case, the main variation in cell voltage occurs along the diluate flow direction, though a fairly important variation is also observed along the concentrate flow direction.

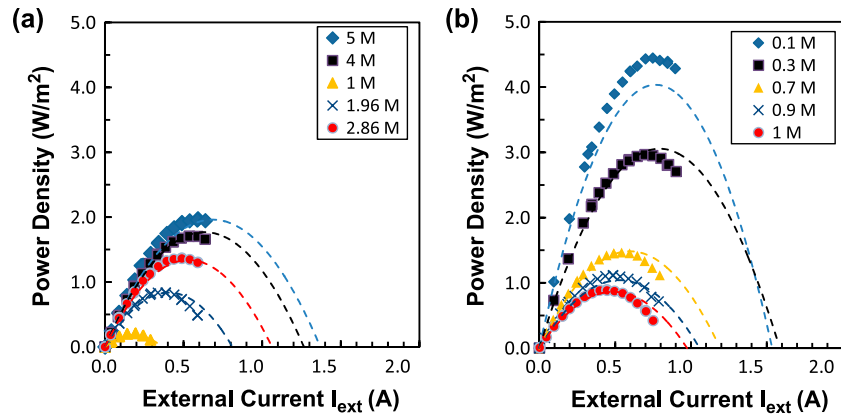


Fig. 4. Effect of (a) HIGH and (b) LOW inlet concentration on Power density. Experimental data (points) and model predictions (curves) for a 50-cells stack equipped with Fujifilm membranes $10 \times 10 \text{ cm}^2$ and $270 \mu\text{m}$ woven spacers; (a) $C_{LOW} = 0.55 \text{ M}$; (b) $C_{HIGH} = 5 \text{ M}$; fluid velocity: 1 cm/s ; $T = 20^\circ\text{C}$.

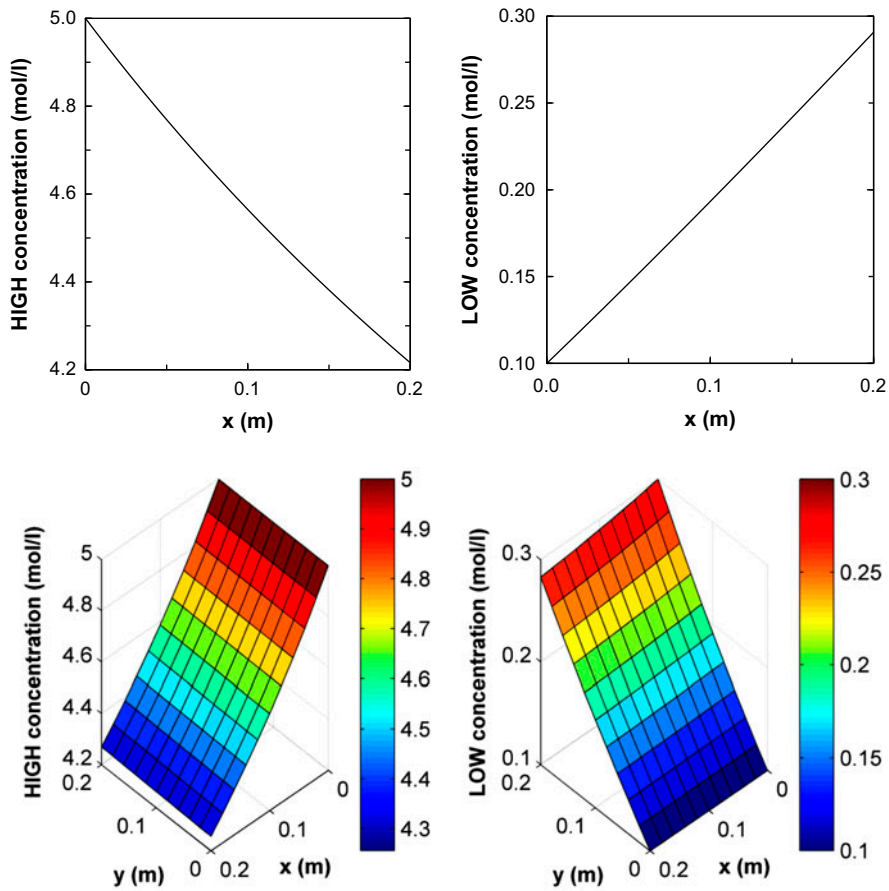


Fig. 5. Concentration profiles within compartments estimated by the previous 1-D co-current model (above, [20]) and by the 2-D cross-flow model (below). Simulations of a $20 \times 20 \text{ cm}^2$ 50 cell pairs stack equipped with Fujifilm membranes, $270 \mu\text{m}$ woven spacers; $C_{HIGH} = 5 \text{ M}$, $C_{LOW} = 0.1 \text{ M}$; fluid velocity: 0.5 cm/s ; $T = 20^\circ\text{C}$.

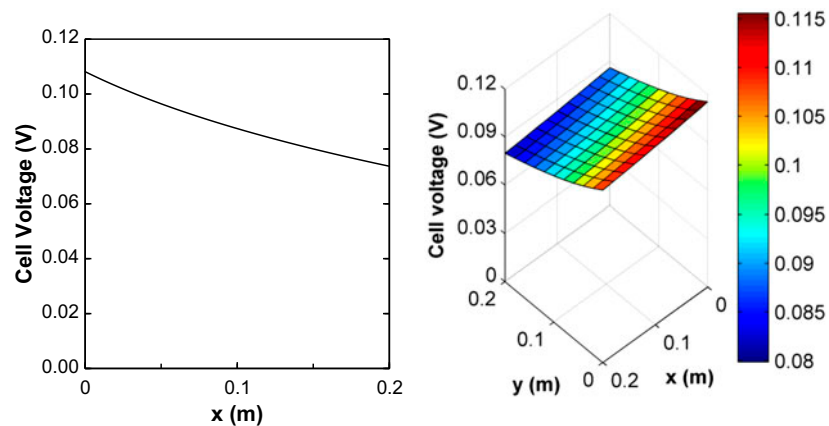


Fig. 6. Voltage profile within a cell pair estimated by the previous 1-D co-current model (left, [20]) and by the 2-D cross-flow model (right). Simulations of a $20 \times 20 \text{ cm}^2$ 50 cell pairs stack equipped with Fujifilm membranes, $270 \mu\text{m}$ woven spacers; $C_{HIGH} = 5 \text{ M}$, $C_{LOW} = 0.1 \text{ M}$; fluid velocity: 0.5 cm/s ; $T = 20^\circ\text{C}$.

3.2. Effect of different path lengths for diluate/concentrate streams

It has been already highlighted that the effect of diluate and concentrate on the overall stack resistance is sensibly different [22]. In order to simulate different path length for diluate and concentrate streams, the aspect ratio of the equipment has been defined as:

$$\text{Aspect Ratio}(AR) = \frac{\text{HIGH path length } (L)}{\text{LOW path length } (b)} \quad (9)$$

According to such definition, an aspect ratio < 1 means a short compartment for concentrate and longer for diluate. The effect of aspect ratio on process performance is shown in Figs. 7 and 8 for a 100 cell pairs

stack. Simulations were carried out assuming alternatively a fixed path length of 20 cm for one of the two streams, and increasing the path length for the other up to five times (i.e. from 20 up to 100 cm). Flow rates of both solutions were adjusted accordingly, in order to keep the same fluid velocity (1 cm/s) inside all channels.

Fig. 7 shows that the power density is negatively affected by a longer path length of the two streams, due to the increased residence time and consequent reduction in the average concentration gradient available. In particular, the increase in the diluate path length leads to a significant reduction in the power density generated. Conversely, a longer path length for concentrate has a weaker effect. In particular, increasing the paths length ratio from 1 (i.e. $20 \times 20 \text{ cm}^2$

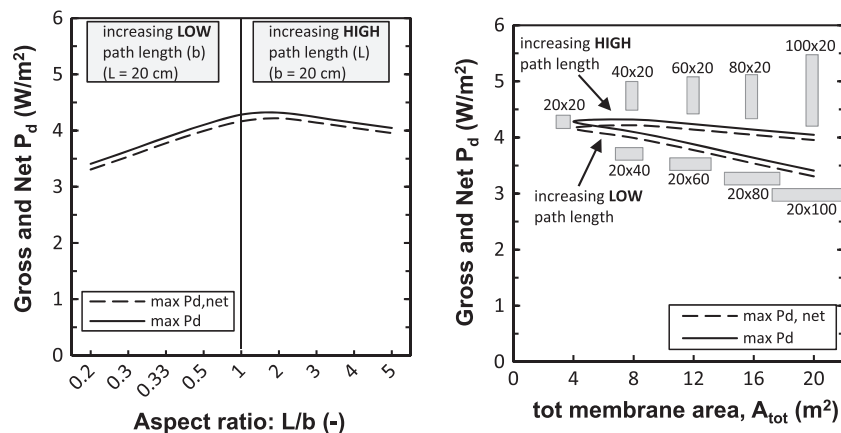


Fig. 7. Influence of aspect ratio on gross and net power density. Simulations of a 100 cell pairs stack equipped with Fujifilm membranes, $270 \mu\text{m}$ woven spacers; $C_{LOW} = 0.1 \text{ M}$, $C_{HIGH} = 5 \text{ M}$; $v_{HIGH} = v_{LOW} = 1 \text{ cm/s}$; $T = 20^\circ\text{C}$. The same model predictions are shown as a function of aspect ratio (left plot) or total membrane area (right plot).

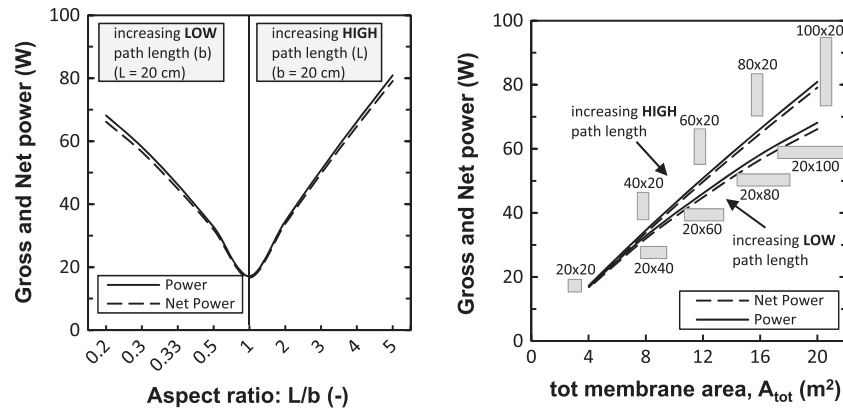


Fig. 8. Influence of aspect ratio on gross and net power. Simulations of a 100 cell pairs stack equipped with Fujifilm membranes, 270 μm woven spacers; $C_{\text{LOW}} = 0.1 \text{ M}$, $C_{\text{HIGH}} = 5 \text{ M}$; $v_{\text{HIGH}} = v_{\text{LOW}} = 1 \text{ cm/s}$; $T = 20^\circ\text{C}$. The same model predictions are shown as a function of aspect ratio (left plot) or total membrane area (right plot).

symmetric stack) up to 5 ($20 \times 100 \text{ cm}^2$ stack), a decrease in the power density of 20 and 7% are predicted by the model for the first and the second case, respectively. A local maximum in the power density is predicted for $\text{AR} = 2$, where the P_d is slightly higher than for symmetrical stack. Such initial increase is likely related to a beneficial effect of the reduced mean concentration of the concentrate stream on membranes permselectivity. On the other hand, the global reduction is clearly related to the average reduction of driving force within the stack. On this basis, increasing the concentrate path length does benefit more the power output in terms of total net power produced (Fig. 8), indicating how the use of asymmetric stack, using a shorter path for diluate, allows to enhance the power output and yield (defined with respect to the *HIGH* feed solution) of a RED process.

3.3. Exploring the optimal operating conditions

3.3.1. Effect of salt concentration

The effect of inlet concentration for both diluate and concentrate has been investigated on a $20 \times 20 \text{ cm}^2$ stack equipped with 100 cell pairs (Fig. 9). It is worth noting that feed concentrations affect also the viscosity of solutions and, therefore, the pressure drops inside the stack. As a consequence, the effect of inlet concentration on net power density is slightly different (Fig. 9(b)).

Interestingly, the maximum power density is achieved by the $20 \times 20 \text{ cm}^2$ stack at inlet concentration of approximately 0.08 and 4.7 M NaCl, which can be identified as optimal solutions for the investigated case. It is worth noting that such conditions lie in a similar concentration range as the one previously identified by the same authors for a $10 \times 10 \text{ cm}^2$ stack

[23]. On the other side, the net power density map (Fig. 9b) shows a zone where negative values are predicted, indicating that the pumping power is greater than the gross power output.

3.3.2. Influence of feed flow rates

Starting from the optimal feed concentration shown in Fig. 9, different conditions were explored in order to find the best flow rates for both solutions. Fig. 10 shows gross and net power density for a $20 \times 20 \text{ cm}^2$ 100-cells stack assuming a fluid velocity ranging from 0.1 up to 3 cm/s for both solutions.

Clearly, the higher the fluid velocity, the higher will be the gross power density (Fig. 10(a)), due to the low residence time for both solutions inside the stack and relevant larger driving forces kept between the membranes. However, it is worth noting that the maximum for the diluate velocity is not achieved at the boundary. In fact, P_d increases until an optimal velocity of about 2.7 cm/s is reached, while for larger values of velocity, P_d decreases again. This is related to the effect of the increase in electrical resistance due to the low conductivity of the solution, generated by extremely small residence times.

On the other side, some interesting results are shown in Fig. 10(b), where the net power density is plotted as a function of *LOW* and *HIGH* fluid velocities. Model predictions show that a maximum net power density of 4.6 W/m^2 can be reached choosing a fluid velocity of 1 cm/s for concentrate and between 2 and 2.5 cm/s for diluate. This ensures high driving forces, but with acceptable pressure drops.

All the results shown so far indicate how the system performance is sensibly affected by diluate

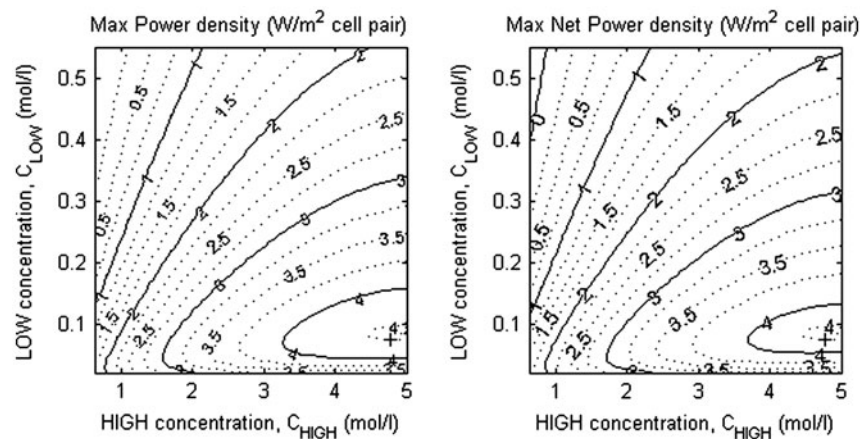


Fig. 9. Effect of the inlet concentration on gross and net power density for a $20\text{ cm} \times 20\text{ cm}$ 100-cells stack, equipped with Fujifilm membranes, $270\text{ }\mu\text{m}$ woven spacers. Feed flow velocity: 1 cm/s ; $T = 20^\circ\text{C}$.

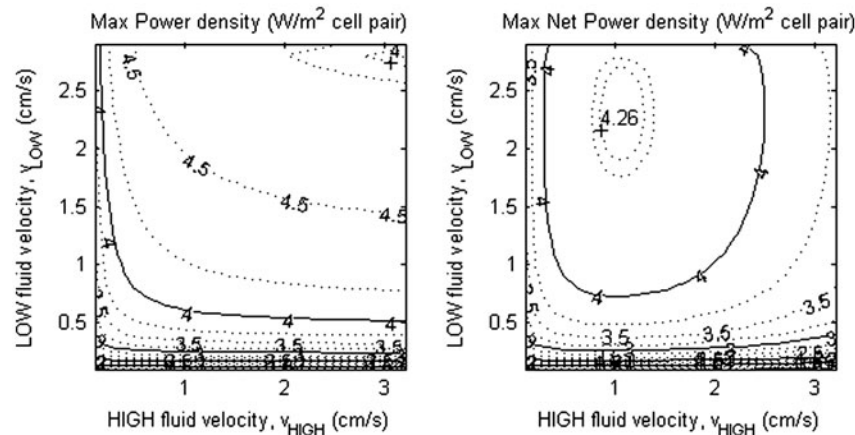


Fig. 10. Effect of channel velocities on gross and net power density for a $20\text{ cm} \times 20\text{ cm}$ 100-cells stack, equipped with Fujifilm membranes, $270\text{ }\mu\text{m}$ woven spacers; $C_{\text{LOW}} = 0.08\text{ M}$, $C_{\text{HIGH}} = 4.7\text{ M}$; $T = 20^\circ\text{C}$.

properties. In order to explore in more detail the optimal operating conditions for a 100-cells stack ($20 \times 20\text{ cm}^2$), a further analysis has been carried out changing both velocity and inlet concentration for the diluate. Results are shown in Fig. 11, where gross and net power density are plotted as a function of the operating conditions for diluate, ranging from 0.1 to 3 cm/s for fluid velocity, and from 0.01 to 0.55 M for inlet concentration. All the simulations were performed changing the concentrate fluid velocity accordingly with the diluate velocity.

Given the assumption of equal fluid velocities for both streams, a maximum net power density of 4.18 W/m^2 is predicted by the model, in conditions slightly different than in the previous cases, i.e. with a fluid velocity of 1.5 cm/s and a *LOW* inlet concentration close to 0.1 M NaCl (Fig. 11(b)).

3.4. Simulation of a pilot-scale unit

In order to simulate a larger RED unit (with reference, in particular, to the prototype unit designed for the operation with saltworks brines in Trapani, Italy, within the REAPower project [24]), a number of different scenarios were taken into account starting from a $22 \times 22\text{ cm}^2$ stack (100 cells) as reference case (Table 1). All scenarios were designed to investigate the effect of scale-up on either symmetric or asymmetric stack design. A concentrated brine of 5 M NaCl and brackish water (0.1 M NaCl) were considered as feed solutions for all cases. When simulating asymmetric stacks, the concentrated brine was always fed to the longer channel, given the better performance registered in the previously reported analysis for such flow configuration.

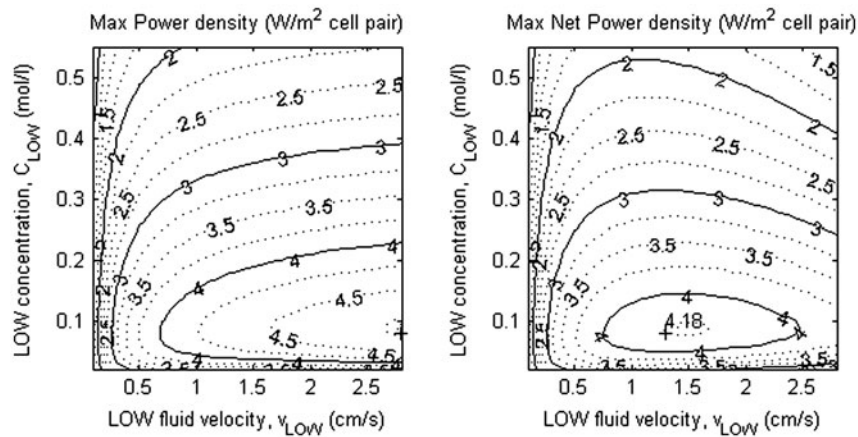


Fig. 11. Gross and net power density as a function of operative conditions (inlet concentration in diluate compartment and fluid velocity). Simulations of a 20 cm × 20 cm 100-cells stack, equipped with Fujifilm membranes, 270 μm woven spacers; $C_{HIGH} = 4.7$ M; $v_{HIGH} = v_{LOW}$; $T = 20^\circ\text{C}$.

Table 1
Summary of simulations carried out on large prototype unit

Scenario #	Membrane size (cm)	No. cell pairs	Total membrane area (m ²)	Description
1	22 × 22	100	4.8	Reference case (small prototype)
2	22 × 22	500	24.2	Larger number of cell pairs
3	44 × 44	500	96.8	Larger symmetric stack
4	22 × 88	500	96.8	Larger asymmetric stack, AR = 4
5	44 × 88	500	193.6	Larger asymmetric stack, AR = 2
6	22 × 88	500	96.8	Asymmetric stack, different velocity ($v_{LOW} = 1$ cm/s, $v_{HIGH} = 2$ cm/s)

Fig. 12 shows the gross and net power density for the investigated scenarios. As expected, the decrease in power density due to the longer HIGH path length is rather negligible. Moreover, increasing the number of cell pairs up to 500 (scenario 2) causes a slight reduction in power density, likely due to the following two counteracting effects: (1) reduction of the influence of blank resistance on the overall performance and (2) increase in stack parasitic currents reducing the power output.

Fig. 13 shows the predicted gross and net power output for the above-mentioned scenarios. In the case of 44 × 88 cm² stack equipped with 500 cell pairs (scenario 5), a power output of almost 900 W has been predicted, which emphasise how the target of 1 kW can be reached with a single stack provided that an active membrane area of 44 × 88 cm² is guaranteed.

3.5. Process simulation of a plant with 3 RED units

The developed process simulator was finally used to describe the operation of a whole RED plant with a

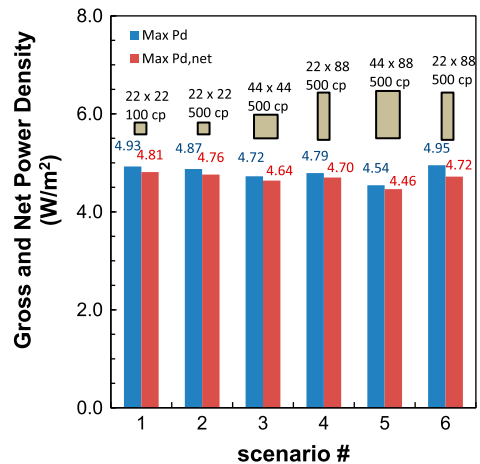


Fig. 12. Gross and net power density for stacks equipped with Fujifilm membranes, 270 μm woven spacers; $C_{LOW} = 0.1$ M; $C_{HIGH} = 5$ M; $v_{LOW} = v_{HIGH} = 1$ cm/s, in scenario no. 6 $v_{LOW} = 2$ cm/s, $v_{HIGH} = 1$ cm/s; $T = 30^\circ\text{C}$.

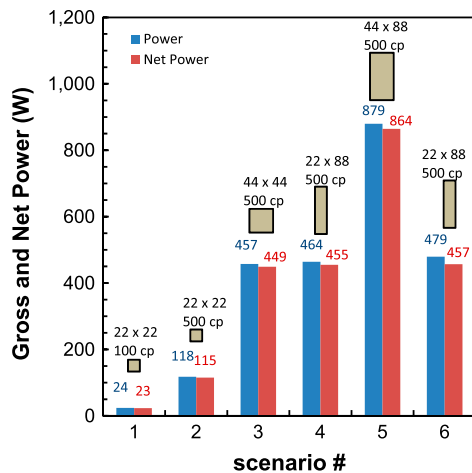


Fig. 13. Gross and net power density for stacks equipped with Fujifilm membranes, 270 μm woven spacers; $C_{LOW}=0.1\text{ M}$; $C_{HIGH}=5\text{ M}$; $v_{LOW}=v_{HIGH}=1\text{ cm/s}$, in scenario no. 6 $v_{LOW}=2\text{ cm/s}$, $v_{HIGH}=1\text{ cm/s}$; $T=30^\circ\text{C}$.

train of three units, each one with a $44 \times 44\text{ cm}^2$ active membrane area and 500 cell pairs. The main goal of this modelling task was to simulate the possible plant layouts to be adopted for the REAPower demonstration plant [24], using concentrated brine and brackish water as feed solutions.

Aside from the stack design, the streams arrangement among the units can significantly affect the overall power output, as well as the performance of each single stack.

In all simulations, the assumption was made of having an HIGH feed flow rate of 29.4 l/min, in order to guarantee the standard internal velocity of 1 cm/s. However, three different scenarios in terms of diluate feed flow rates were investigated to analyse the effect of different feed rates availability in the real installation site. In particular, the flow rates of 20 l/min, 29.4 l/min (as in the HIGH channels) and 40 l/min were set in the three simulation sets. Moreover, the diluate feed concentration was set to 0.03 M, according to the real availability of brackish water in the prototype installation site.

As previously shown, the residence time of concentrated brine has been found not to be dramatic for process performance. For this reason, a serial arrangement among units was adopted for the concentrate. Conversely, a number of possible distribution paths have been analysed for the diluate. In Fig. 14, the three most promising configurations are shown, namely:

- *Layout 1 (serial arrangement, Fig. 14(a)).* Three stacks are fed in series for both diluate and

concentrate, with a recycle for the diluate in the first stage, allowing the control of fluid velocity of 1 cm/s inside all channels of the first stack, even if the availability of brackish water is low. This arrangement also guarantees in the first stack a more uniform concentration in the dilute compartment, in a range closer to the previously identified optimal concentration.

- *Layout 2 (parallel arrangement, Fig. 14(b)).* All stacks are fed in series for the concentrate stream, and in parallel for the diluate, thus requiring a partial recycle of the exiting dilute stream in order to operate all the three stacks with the standard velocity of 1 cm/s. This configuration ensures more homogeneous driving force for all units.
- *Layout 3 (parallel–serial arrangement, Fig. 14(c)).* this hybrid configuration provides a parallel feed for diluate into the first two stacks, using the overall outlet to feed the third unit, where the fluid velocity will be much larger than in standard conditions.

The implemented flowsheet in gPROMS Model Builder environment [25] for the first layout is shown in Fig. 15.

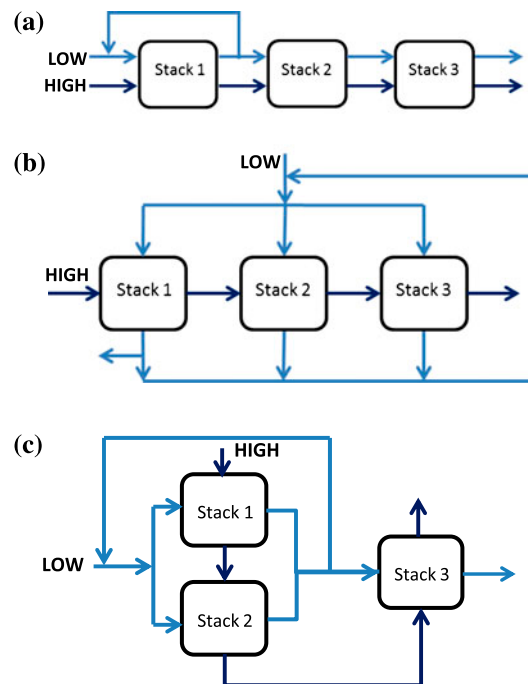


Fig. 14. Investigated layouts for streams arrangements. (a) Serial arrangement; (b) parallel arrangement; (c) parallel–serial arrangement.

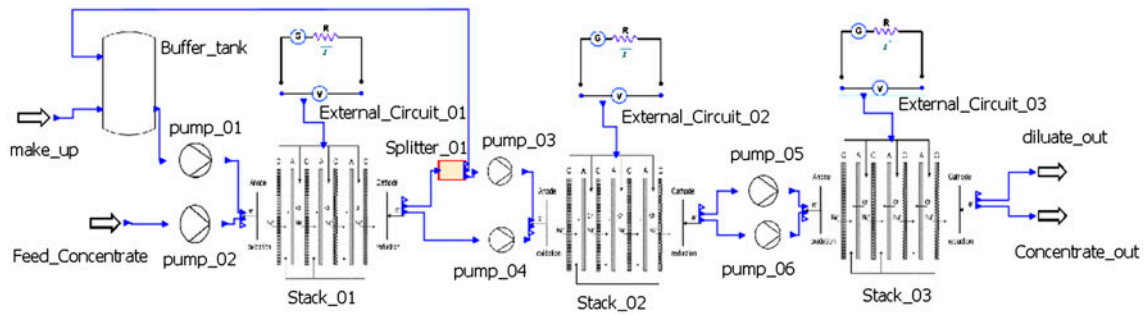


Fig. 15. Implemented flowsheet for 3 RED units.

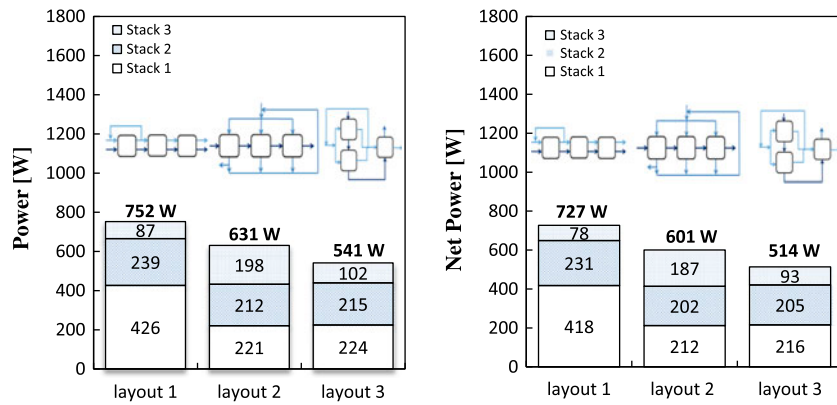


Fig. 16. Gross and net power of three stacks (500 cells) equipped with Fujifilm membranes $44 \times 44 \text{ cm}^2$ and $270 \mu\text{m}$ woven spacers, in layout 1: serial; layout 2: parallel; layout 3: parallel-serial for diluate feed; $C_{HIGH} = 5 \text{ M}$; $Q_{HIGH} = 29.41/\text{min}$; make-up of brackish water, $Q_{MU} = 201/\text{min}$, $C_{MU} = 0.03 \text{ M}$.

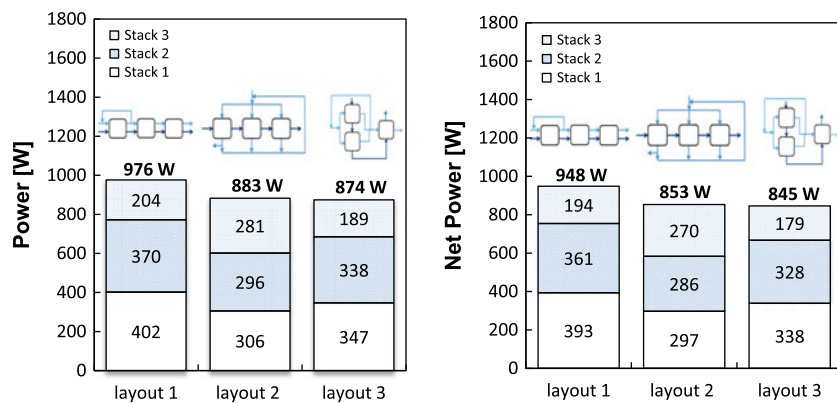


Fig. 17. Gross and net power of 3 stacks (500 cells) equipped with Fujifilm membranes $44 \times 44 \text{ cm}$ and $270 \mu\text{m}$ woven spacers, in layout 1: serial; layout 2: parallel; layout 3: parallel-serial for diluate feed; $C_{HIGH} = 5 \text{ M}$; $Q_{HIGH} = 29.41/\text{min}$; make-up of brackish water, $Q_{MU} = 29.41/\text{min}$, $C_{MU} = 0.03 \text{ M}$.

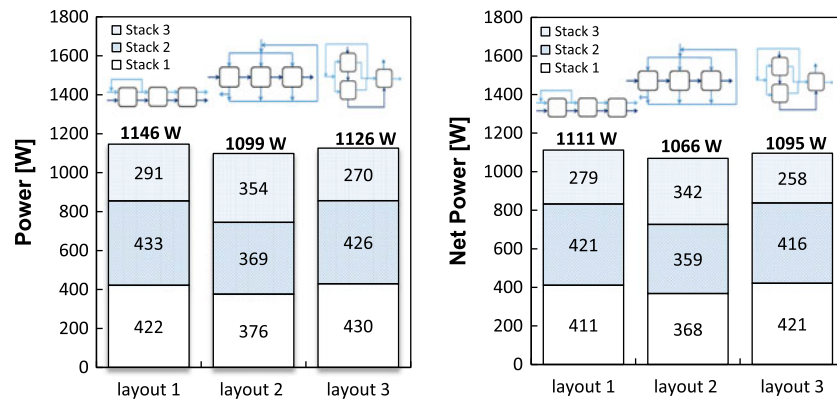


Fig. 18. Gross and net power of 3 stacks (500 cells) equipped with Fujifilm membranes $44 \times 44 \text{ cm}^2$ and $270 \mu\text{m}$ woven spacers, in layout 1: serial; layout 2: parallel; layout 3: parallel-serial for diluate feed; $C_{\text{HIGH}} = 5 \text{ M}$; $Q_{\text{HIGH}} = 29.41 \text{ l/min}$; make-up of brackish water, $Q_{\text{MU}} = 401 \text{ l/min}$, $C_{\text{MU}} = 0.03 \text{ M}$.

The first set of model predictions, relevant to the case of diluate feed flow rate of 20 l/min , are reported in Fig. 16.

For layout 1 (serial arrangement), a make-up of 20 l/min of brackish water is not enough to guarantee a velocity of 1 cm/s in all channels. For this reason, a recycle of the outlet diluate is required at least after the first stack. It is worth noting that layout 2 (parallel arrangement) is clearly the optimal configuration to ensure equal performance for all stacks. Nonetheless, layout 1 (serial arrangement) gives a higher power output (752 W), while the layouts 2 and 3 can provide (with 3 stacks) the same power output generated by the first 2 stacks in layout 1.

In order to feed the plant with no recycle and keep a fluid velocity of 1 cm/s in all channels, the required brackish water flow rate is 29.41 l/min . Fig. 17 shows model predictions for the investigated plant layouts assuming the availability of 29.41 l/min of brackish water as make-up to the plant.

An increase in the diluate make-up allowed to reach a power output of 976 W for layout 1 (Fig. 17). Moreover, a higher make-up of brackish water gives minor differences among the layouts in terms of power output, significantly improving the performances of layouts 2 and 3.

The availability of brackish water is a key factor for the plant performance. Assuming to double the original amount of brackish water available, the process simulator was eventually used to predict the plant operation with a make-up of brackish water of 401 l/min (Fig. 18).

A brackish water availability of 401 l/min would allow to reach more than 1 kW with all of the investigated plant layout. Interestingly, for layout 1, the power produced from the second stage (433 W) is slightly higher than the power from the first stage

(422 W). This is because in the second stage, the diluate inlet concentration is closer to its optimal value, as previously shown by the parametric analysis (Fig. 10).

4. Conclusions

This work presents a new process simulator for a RED plant using sea/brackish water and concentrated brines as feed solutions. Starting from a previous work by the same authors, a new model was implemented for simulating the performance of a RED unit with cross-flow arrangement. Regarding the stack design, the possibility of using asymmetric stack has been addressed, being the model able to simulate different flow path lengths for dilute and concentrate streams, adopting a $20 \times 20 \text{ cm}^2$ stack with 100 cell pairs as reference case. Model predictions showed how increasing the aspect ratio from 1 (i.e. $20 \times 20 \text{ cm}^2$ symmetric stack) up to 5 ($20 \times 100 \text{ cm}^2$ stack), a decrease from 7 to 20% in the power density is registered, with larger effects observed when increasing the diluate channel length. On the other side, increasing the concentrate path length enhances almost proportionally the power output and the overall process yield (defined with respect to the concentrate stream) achieved.

An optimisation analysis has been performed in order to identify optimal operating conditions for a $20 \times 20 \text{ cm}^2$ stack in terms of optimal inlet feed concentration and velocities, highlighting the dominant influence of diluate compartment conditions on the overall unit performance.

Finally, simulations were performed to predict the behaviour of a larger prototype plant, being this a preliminary analysis for the construction of a demonstration plant to be installed in Trapani (Italy) as a final deliverable of the REAPower project [21]. A number

of possible layouts have been presented; connecting 3 RED units equipped with 500 cells pairs of $44 \times 44 \text{ cm}^2$ active membrane area. Three different conditions were considered in terms of availability of diluate feed. Interestingly, in the case of low availability of brackish water (20 l/min), a serial arrangement is preferable, with two stacks in series providing practically the same power output as three stacks differently connected in the other two layouts. However, assuming an availability of brackish water of 40 l/min, simulations indicate a much closer performance between the three layouts, allowing to reach in all cases more than 1 kW power output.

Acknowledgements

This work has been performed within the REA-Power (Reverse Electrodialysis Alternative Power production) project [21], funded by the EU-FP7 programme (Project number: 256736).

References

- [1] G.Z. Ramon, Membrane-based production of salinity-gradient power, *Energy Environ. Sci.* 4 (2011) 4423–4434.
- [2] J.W. Post, J. Veerman, H.V.M. Hamelers, G.J.W. Euverink, S.J. Metz, K. Nijmeijer, C.J.N. Buisman, Salinity-gradient power: Evaluation of pressure-retarded osmosis and reverse electrodialysis, *J. Membr. Sci.* 288 (2007) 218–230.
- [3] D.A. Vermaas, J. Veerman, N.Y. Yip, M. Elimelech, M. Saakes, K. Nijmeijer, High efficiency in energy generation from salinity gradients with reverse electrodialysis, *ACS Sustainable Chem. Eng.* 1 (2013) 1295–1302.
- [4] D. Brogioli, Extracting renewable energy from a salinity difference using a capacitor, *Phys. Rev. Lett.* 103 (2009) 058501(4).
- [5] B.B. Sales, M. Saakes, J.W. Post, C.J.N. Buisman, P.M. Biesheuvel, H.V.M. Hamelers, Direct power production from a water salinity difference in a membrane-modified supercapacitor flow cell, *Environ. Sci. Technol.* 44 (2010) 5661–5665.
- [6] A. Daniilidis, R. Herber, D.A. Vermaas, Upscale potential and financial feasibility of a reverse electrodialysis power plant, *Appl. Energy* 119 (2014) 257–265.
- [7] H. Strathmann, *Ion-exchange Membrane Separation Processes*, vol. 9, Elsevier Science, Amsterdam, 2004.
- [8] L. Gurreri, A. Tamburini, A. Cipollina, G. Micale, M. Ciofalo, CFD simulation of mass transfer phenomena in spacer filled channels for reverse electrodialysis applications, *Chem. Eng. Trans.* 32 (2013) 1879–1884.
- [9] L. Gurreri, A. Tamburini, A. Cipollina, G. Micale, M. Ciofalo, CFD prediction of concentration polarization phenomena in spacer-filled channels for reverse electrodialysis, *J. Membr. Sci.* 468 (2014) 133–148.
- [10] J. Veerman, J.W. Post, M. Saakes, S.J. Metz, G.J. Harmsen, Reducing power losses caused by ionic shortcut currents in reverse electrodialysis stacks by a validated model, *J. Membr. Sci.* 310 (2008) 418–430.
- [11] R.E. Lacey, Energy by reverse electrodialysis, *Ocean Eng.* 7 (1980) 1–47.
- [12] E. Brauns, Salinity gradient power by reverse electrodialysis: Effect of model parameters on electrical power output, *Desalination* 237 (2009) 378–391.
- [13] J. Veerman, M. Saakes, S.J. Metz, G.J. Harmsen, Reverse electrodialysis: A validated process model for design and optimization, *Chem. Eng. J.* 166 (2011) 256–268.
- [14] J.W. Post, H.V.M. Hamelers, C.J.N. Buisman, Energy recovery from controlled mixing salt and fresh water with a reverse electrodialysis system, *Environ. Sci. Technol.* 42 (2008) 5785–5790.
- [15] D.A. Vermaas, E. Guler, M. Saakes, K. Nijmeijer, Theoretical power density from salinity gradients using reverse electrodialysis, *Energy Procedia* 20 (2012) 170–184.
- [16] A. Tamburini, G. La Barbera, A. Cipollina, M. Ciofalo, G. Micale, CFD simulation of channels for direct and reverse electrodialysis, *Desalin. Water Treat.* 48 (2012) 370–389.
- [17] L. Gurreri, A. Tamburini, A. Cipollina, G. Micale, CFD analysis of the fluid flow behavior in a reverse electrodialysis, *Desalin. Water Treat.* 48 (2012) 390–403.
- [18] L. Gurreri, M. Ciofalo, A. Cipollina, A. Tamburini, W. Van Baak, G. Micale, CFD modelling of profiled-membrane channels for reverse electrodialysis, *Desalin. Water Treat.* (in press). doi: 10.1080/19443994.2014.940651.
- [19] M. Tedesco, A. Cipollina, A. Tamburini, W. van Baak, G. Micale, Modelling the reverse electrodialysis process with seawater and concentrated brines, *Desalin. Water Treat.* 49 (2012) 404–424.
- [20] M. Tedesco, A. Cipollina, A. Tamburini, I.D.L. Bogle, G. Micale, A simulation tool for analysis and design of Reverse Electrodialysis using concentrated brines, *Chem. Eng. Res. Des.* (in press). doi:10.1016/j.cherd.2014.05.009.
- [21] K.M. Hangos, I.T. Cameron, *Process Modelling and Model Analysis*, vol. 4, Academic Press, 2001.
- [22] A. Daniilidis, D.A.A. Vermaas, R. Herber, K. Nijmeijer, Experimentally obtainable energy from mixing river water, seawater or brines with reverse electrodialysis, *Renewable Energy* 64 (2014) 123–131.
- [23] M. Tedesco, A. Cipollina, A. Tamburini, G. Micale, J. Helsen, M. Papapetrou, Reapower: Use of desalination brine for power production through reverse electrodialysis, *Desalin. Water Treat.* (in press). doi:10.1080/19443994.2014.934102.
- [24] www.reapower.eu. Copyright 2010 REAPower/WIP Munich.
- [25] “gPROMS Model Builder 3.3.1”, Process Systems Engineering, 2010.